Nanoscale Structural and Electronic Properties of Ultrathin Blends of Two Polyaromatic Molecules: A Kelvin Probe Force Microscopy Investigation

ARTICLE *in* CHEMPHYSCHEM · APRIL 2006

Impact Factor: 3.42 · DOI: 10.1002/cphc.200500480 · Source: PubMed

8 AUTHORS, INCLUDING:

Vincenzo Palermo
Italian National Research Council
130 PUBLICATIONS **2,576** CITATIONS
SEE PROFILE

Matteo Palma
Queen Mary, University of London
28 PUBLICATIONS **605** CITATIONS
SEE PROFILE

Andreas Herrmann
University of Groningen
152 PUBLICATIONS **4,496** CITATIONS
SEE PROFILE

Paolo Samorì
University of Strasbourg
272 PUBLICATIONS **7,338** CITATIONS
SEE PROFILE

DOI: 10.1002/cphc.200500480

Nanoscale Structural and Electronic Properties of Ultrathin Blends of Two Polyaromatic Molecules: A Kelvin Probe Force Microscopy Investigation

Vincenzo Palermo,[a] Susanna Morelli,[a] Matteo Palma,[b] Christopher Simpson,[c] Fabian Nolde,[c] Andreas Herrmann,[c] Klaus Müllen,*[c] and Paolo Samorì*[a, b]

We describe a Kelvin Probe Force Microscopy (KPFM) study on the morphological and electronic properties of complex mono and bi-molecular ultrathin films self-assembled on mica. These architectures are made up from an electron-donor (D), a synthetic all-benzenoid polycyclic aromatic hydrocarbon, and an electron-acceptor (A), perylene-bis-dicarboximide. The former molecule self-assembles into fibers in single component films, while the latter molecule forms discontinuous layers. Taking advantage of the different solubility and self-organizing properties of the A and D molecules, multicomponent ultrathin films characterized by nanoscale phase segregated fibers of D embedded in a discontinuous layer of A are formed. The direct estimation of the surface potential, and consequently the local workfunction from KPFM images allow a comparison of the local electronic properties of the blend with those of the monocomponent films. A change in the average workfunction values of the A and D nanostructures in the blend occurs which is primarily caused by the intimate contact between the two components and the molecular order within the nanostructure self-assembled at the surface. Additional roles can be ascribed to the molecular packing density, to the presence of defects in the film, to the different conformation of the aliphatic peripheral chains that might cover the conjugated core and to the long-range nature of the electrostatic interactions employed to map the surface by KPFM limiting the spatial and potential resolution. The local workfunction studies of heterojunctions can be of help to tune the electronic properties of active multicomponent films, which is crucial for the fabrication of efficient organic electronic devices as solar cells.

Introduction

The performance of (opto)electronic devices based on π-conjugated molecules strongly depends on the interplay between the structural arrangement of the components at the supramolecular level and their (opto)electronic properties.[1–3] Organic solar cells can be fabricated by using a heterojunction as the active layer, that is, two interfaced materials with an electron acceptor (A) and donor (D) character.[4,5] The electronic interaction between the two phases generates an electric field at their interface. Such a field can split photogenerated holes and electrons, triggering their migration to the cathode and anode, respectively, thus leading to the generation of an electrical current.[6] A high contact area between the two phases and a continuous path of both A and D materials to the electrodes are therefore required,[7,8] as the probability of an electron–hole pair, that is, exciton, to diffuse to the interface and split is directly proportional to the interfacial area and to the distance the exciton has to travel to reach the interface.[5] Thus, the formation of a nanostructure possessing such characteristics and the understanding of its electronic properties on the nanoscale, is an essential prerequisite for the development of efficient organic solar cells prototypes.

The electronic structure of organic thin films is usually investigated by X-ray and ultraviolet photoelectron spectroscopy (XPS and UPS).[9] As the measurements performed with these techniques are typically averaged over a microscopic area, the application of these methods is often not appropriate for the study of discontinuous nanostructures.

Kelvin probe force microscopy (KPFM)[10,11] is a chemically sensitive, contactless technique developed as a modification of scanning force microscopy (SFM).[12] By mapping the electrostatic interactions between a conductive tip and the sample during the scan, KPFM allows regions of higher or lower poten-

[a] *Dr. V. Palermo, S. Morelli, Dr. P. Samorì*
Istituto per la Sintesi Organica e la Fotoreattività
Consiglio Nazionale delle Ricerche
via Gobetti 101, 40129 Bologna (Italy)
Fax: (+39) 051-6399844
E-mail: samori@isof.cnr.it

[b] *M. Palma, Dr. P. Samorì*
Nanochemistry Laboratory
Institut de Science et d'Ingénierie Supramoléculaires (ISIS)
Université Louis Pasteur
8, allée Gaspard Monge , 67083 Strasbourg (France)

[c] *Dr. C. Simpson, F. Nolde, Dr. A. Herrmann, Prof. Dr. K. Müllen*
Max-Planck Institute for Polymer Research
Ackermannweg 10, 55124 Mainz (Germany)
Fax: (+49) 6131-379350
E-mail: muellen@mpip-mainz.mpg.de

Supporting information for this article is available on the WWW under http://www.chemphyschem.org or from the author.

tial on the sample surface to be highlighted. In the absence of any external applied bias, this measured potential difference between the tip and sample corresponds to the difference in workfunction ϕ, that is, the energy difference between the vacuum level and Fermi level in a solid.[13]

By calibrating the tip with a sample having a well-known workfunction, such as graphite, the workfunction of different nanostructures on the sample surface can be determined with a potential resolution of a few millivolts. KPFM has been extensively utilized to study inorganic semiconductors,[14] carbon nanotubes,[15] organic thin films including chemisorbed self-assembled monolayers of both alkanethiols on Au[16] and phenylacetylene on SiO_2,[17] as well as Langmuir–Blodgett monolayers of hexa-*peri*-hexabenzocoronene on SiO_2,[18] with a lateral resolution down to some tens of nanometers. Moreover, it has provided insight into the electrostatic potential decay in field-effect transistors (FETs) based on oligo-[19] and poly-alkylthiophenes[20] as well as pentacenes.[21] The suitability of KPFM to explore the local electronic properties of multicomponent films for photovoltaic applications has recently been proven by studying organic heterojunctions consisting of thick ($h = 50$–100 nm) amorphous blend films of two polymers[22] and polymer/fullerenes on a sub-micrometer scale.[23] It is still a great challenge to unravel the local electronic properties of nanoscale phase-segregated acceptor–donor blends in films with a sub-monolayer thickness.

Herein we report a KPFM structural and electronic characterization of ultrathin A–D blend films featuring distinct nanoscale phase segregation between the two building blocks. These results are compared to those obtained on single component ultrathin films prepared from either the A or the D molecule.

We have utilized a giant, alkylated all-benzenoid polycyclic aromatic hydrocarbon (PAH; octa-3,7,11,15-tetramethylhexadecyl C132, named C132-C_{16} hereafter) as the electron donor and a perylene (*N*,*N*′-bis(1-ethylpropyl)-3,4,9,10-perylene-bis-dicarboximide, PDI) as an electron acceptor (see Figures 1a and 1b). The former, which is, to-date, the largest soluble nanographene molecule, combines a relatively easy solution processability[24,25] with a high charge-carrier mobility in the columnar mesophase[26] over a broad temperature range from well under room temperature to more than 300 °C. While the unsubstituted C132 was found by scanning tunneling microscopy to self-assemble into crystalline monolayers,[27] angle-resolved ultraviolet photoelectron spectroscopy revealed a well-defined electronic structure within the C132-C_{16} film.[28] On the other hand, PDI forms ordered architectures on surfaces[29–33] that exhibit a high electron mobility, qualifying them as a promising class of n-channel conductors for organic thin film transistors (OTFTs).[34] Moreover, when blended with liquid-crystalline donor molecules, they can be used to fabricate high-efficiency heterojunctions.[35] Owing to their absorption maxima in the relevant area of the solar spectrum (between 525 and 550 nm), the combination of these two molecules are also well suited for the harvesting of a significant portion of energy from this source.

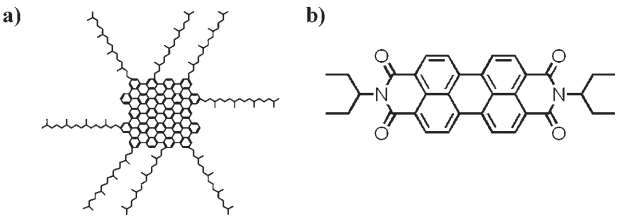

Figure 1. Chemical formula of a) C132-C_{16} and b) PDI.

Results

Figure 2a shows a SFM image of a C132-C_{16} film prepared by dipping a mica substrate in a 5×10^{-7} mol L^{-1} solution in 1,2,4-trichlorobenzene (TCB). It reveals fibers with a constant cross-section forming a continuous network on the surface. The fibers' true width, corrected for the tip broadening,[36] is $w = (56 \pm 25)$ nm, their height is $h = (4 \pm 1)$ nm, and their length exceeds 5 μm. In between the fibers, the surface exhibits a few randomly distributed clusters (black arrows), preferentially located in the fibers' proximity. Given the well-known tendency of conjugated molecules bearing aliphatic side-groups to pack "edge-on" on the basal plane of the insulating mica surface, also because of the different hydrophobic and hydrophilic

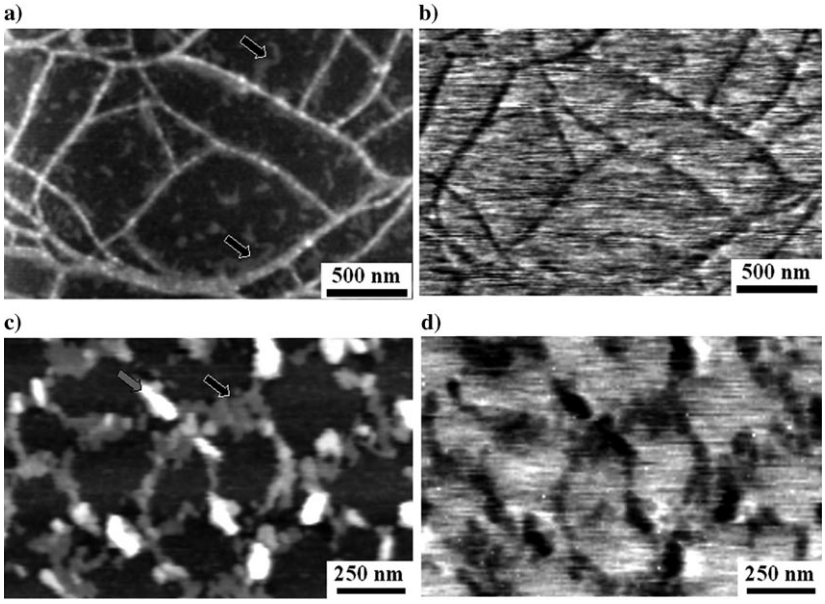

Figure 2. a) SFM topography and b) KPFM image of C132-C_{16} fibers adsorbed on mica. c) SFM topography and d) KPFM image of a PDI discontinuous layer on mica. *Z*-scales: a) 13 nm c) 7 nm.

character of the admolecule and of the substrate,[36] together with the propensity of all-benzenoid PAHs to form columnar discotic phases,[25] it is suggested that the fibers consist of stacks of C132-C_{16} molecules arranged "edge-on" on the surface, similar to previous observations with smaller PAHs, that is, alkylated hexa-*peri*-hexabenzocoronenes.[37] The C132-C_{16} molecular diameter ranges from 2.2 to 6.2 nm (if one either disregards the alkyl side-chains or considers them in their fully extended conformation), so the fibers can be composed of bundles of several molecule-wide columns. This is confirmed by the observation of fibers with smaller cross-sections (see Supporting Information), even down to $\approx$25 nm.

As SFM typically offers just a topographical map of the surface, in order to gain information on the local electronic properties of the surface, the study was extended to KPFM measurements. The KPFM image of the C132-C_{16} film is shown in Figure 2b. A high lateral resolution in the KPFM measurement made it possible to resolve the supramolecular fibers of C132-C_{16} with a spatial resolution of a few nanometers, as confirmed by comparing the KPFM image to the simultaneously recorded topographical SFM image. In our experiments, we used a p-type silicon tip and a freshly cleaved highly oriented pyrolytic graphite (HOPG) reference sample for the setup calibration. The HOPG workfunction in air amounts to 4.65 eV.[14] We measured a contact potential of a freshly cleaved HOPG (ZYH grade, Advanced Ceramics, USA) as: $\Delta V_{(\mathrm{tip-HOPG})} = (0.69 \pm 0.02)$ V. From this value, we determined the silicon tip workfunction: $\phi_{\mathrm{tip}} = \phi_{\mathrm{HOPG}} + \Delta\phi_{(\mathrm{tip-HOPG})} = (5.34 \pm 0.02)$ eV, which is significantly higher than both that tabulated for a p-type silicon, (4.85 ± 0.05) eV[38] and that of other similar tips previously used in our lab.[39] Such a difference is probably due to the complex geometrical shape of the tip and to the partially uncontrollable nature of the native oxide layer. After calibration, other surfaces with a well-known workfunction, such as silicon and gold, were measured to attest the reliability of the methodology, following the procedure we have recently reported.[39] From the potential profiles in the KPFM images, it was possible to determine the ϕ for the C132-C_{16} fibers. The fibers exhibited a contact potential of $\Delta\phi_{(\mathrm{tip-C132})} = (2.14 \pm 0.04)$ eV. Consequently the workfunction value was determined to be $\phi_{\mathrm{C132}} = \phi_{\mathrm{tip}} - \Delta\phi_{(\mathrm{tip-C132})} = (5.34 - 2.14)$ eV $= (3.20 \pm 0.06)$ eV.

It is fair to note that the fibers possess a darker contrast when compared to the underlying mica substrate. Although it has been demonstrated that KPFM can be applied to both semiconducting and insulating substrates,[13,40] the KPFM signal for the electrically insulating mica cannot be correlated to a workfunction value, owing to its ionic nature. In general, it seems that the contact potential measured on the insulating mica substrate fluctuates. The mica substrate can thus exhibit a higher or a lower surface potential with respect to the organic material, depending on the experimental conditions; in particular, important roles can be expected to be played by the humidity and the density of potassium ions existing on the freshly cleaved muscovite mica surface.[41] Thus, a higher or a lower surface potential of the mica substrate can generate a darker or a brighter contrast of the organic adsorbate in the KPFM image, respectively. It is noteworthy that this contrast appears to be poorly related to the absolute measurement of the workfunction of the organic adsorbate, as the measured potential for the organic adlayer mostly depends on the difference in workfunction between the tip (calibrated versus graphite) and the organic architecture.

Current activity in our laboratories is addressed towards a better understanding of the quantitative contact potential measured by KPFM, taking into account the polarizability of the organic adsorbate induced by the charged tip.

SFM images of a neat film of PDI (Figure 2c) reveal a discontinuous irregular layer (black arrow) sometimes coated by small crystallites of irregular shapes (grey arrow). The thickness of the layer amounts to $\approx$2 nm, in good agreement with the molecular size (when considering the ethyl-propyl end-groups are fully extended). The related KPFM image is displayed in Figure 2d. It also shows a good lateral resolution, allowing the identification of both the irregular thin layer and the single crystallites on the surface. From the profiles of the KPFM image, the local ϕ of the PDI layer was estimated to be (3.80 ± 0.06) eV.

Owing to its markedly high tendency to aggregate into clusters, the solubility of C132-C_{16} in most organic solvents is low. To promote its solubilization, and therefore permit its self-assembly from solution into fibers at surfaces, we exploited a poorly volatile solvent, TCB, at high temperature. Low solubility, which usually represents a drawback for the processing of such molecules, can be an advantage in a two-step deposition. PDI can be added on the fibers by spin-coating from a solution made with a solvent in which C132-C_{16} is barely soluble, such as chloroform.

Thus, owing to the different self-assembly behavior and solubility of C132-C_{16} and PDI, we consecutively deposited the two components on mica by first dipping a freshly cleaved mica slide in a 5×10^{-7} mol L^{-1} solution of C132-C_{16} in TCB and then spin-coating on top a 10^{-3} mol L^{-1} solution of PDI in $CHCl_3$. The SFM image in Figure 3a exhibits a complex morphology comprising both fibers and layers. It is worth pointing out, that under the same deposition conditions (of concentration, solvent type, and temperature), C132-C_{16} and PDI were deposited in neat films on separate substrates (see Figures 2a and 2c, respectively) and on the same substrate, consecutively (see Figure 3). The use of a two-step process makes it possible to tune independently the deposition conditions of each molecule, thus improving the overall control of the film formation. Notably, the architecture shown in Figure 3a was found to be stable on the time frame of several days, as no structural rearrangement was observed. The widths (56 ± 12) nm of the C132-C_{16} fibers are very similar in the neat and in the blend film. The height of the fibers in the blend films is (7 ± 2) nm, which is almost double that of the single component films of C132-C_{16}. This different thickness is most likely to be due to a coating of the C132-C_{16} fibers with a PDI layer. This is even more evident for some C132-C_{16} fibers that are unambiguously covered by the PDI layer (black arrows Figure 3a). This coating enables intimate contact between A and D.

The C132-C_{16} fibers template the self-assembly of PDI at surfaces, as evidenced by the different arrangements of the PDI

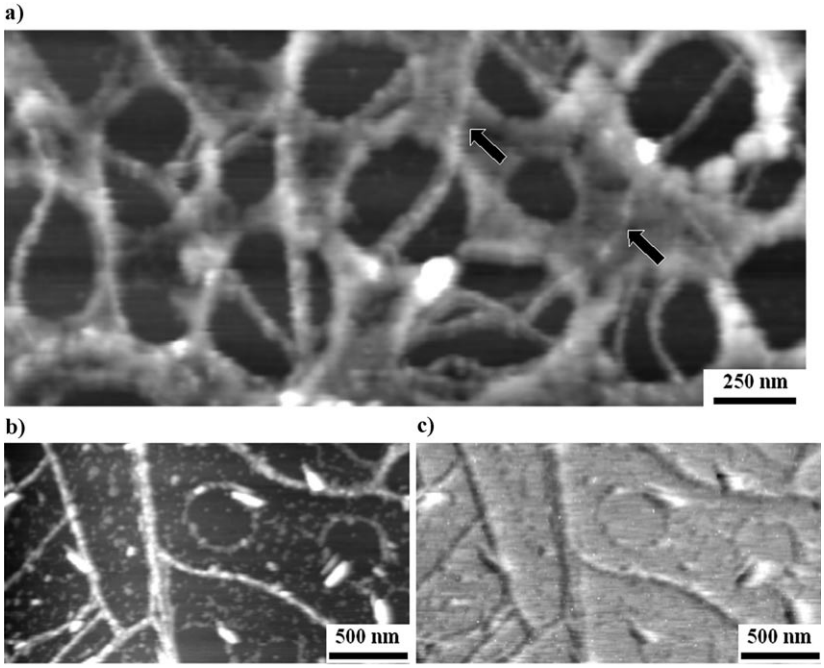

Figure 3. a) and b) SFM topography and c) KPFM image of a C132-C_{16}/PDI blend ultrathin film. (b) and (c) were recorded simultaneously. *Z*-scales: a) 13 nm b) 15 nm.

observed in the monocomponent film (Figure 2c) and in the blend (Figure 3a). In the blend, the PDI does not assemble in small crystallites of irregular shape, but rather it forms layers bearing circular holes, with the layer between the holes being more or less thick and continuous (Figures 3a and 3b). The presence of holes suggests that dewetting plays a fundamental role in surface rearrangement.[42] While the PDI layer's thickness in the neat film was 2 nm, in the blends it was more irregular and ranged from 5 to 10 nm. This can be explained by taking into account the fact that, after spin coating, a thin wet layer of the PDI solution in $CHCl_3$ is placed on the surface. If the surface is the atomically flat neat mica, the evaporation is more uniform, thus allowing the formation of the crystallites and of the thin layer. On the other hand, the wettability of the samples to a PDI solution in $CHCl_3$ is different when the substrate exposes the hydrophobic C132-C_{16} fibers instead of the hydrophilic mica. This, together with the effect determined by the different surface topology in the two cases, perturbs the drying-up of the solvent, and eventually induces an irregular dewetting of the solution on the surface. Because of the dewetting, the liquid layer will break first where there are corresponding defects, irregularities, or sharp points of the surface, thus creating circular holes leading to the surface shown in Figure 3. A more detailed model for the dewetting mechanism has previously been reported.[43] The uncoated circular patches, typical of self-assembly at surfaces governed by dewetting, can eventually enlarge and coalesce, depending on the solvent evaporation rate and molecular reorganization, leading to either an irregular network or isolated clusters.[42]

KPFM made it possible to resolve simultaneously the C132-C_{16} fibers and the PDI layers in the blend with a few nanometers lateral resolution (Figure 3c). The ϕ of C132-C_{16} in the blend was (3.5 ± 0.04) eV, while that of PDI layers amounted to (3.6 ± 0.04) eV. The difference between the two workfunctions decreased by about 0.5 eV. This can be ascribed to many factors, including the presence of interactions between the two nanostructures and the molecular order within an architecture adsorbed at surfaces, which determines a different delocalization of the electrons along the π-stacks. Additional important roles are played by the molecular packing density, the presence of defects in the film, and the different conformation of the aliphatic peripheral chains that might cover the conjugated core, as we recently reported.[39] Furthermore, it is worth noting that a direct contribution of the substrate to the electrostatic interaction between the tip and surface as measured by KPFM can also be possible.[44]

Discussion

The combination of the results of topography and surface potential measurements obtained by KPFM provides an insight into the structure and composition of the blend. Although the C132-C_{16} molecule exhibits poor solubility in $CHCl_3$, rearrangement at the (sub-)molecular scale of the C132-C_{16} fibers can take place during the PDI solution deposition. In particular, the aliphatic side-chains on the external shell of the fibers' surface are likely to rearrange upon exposure to $CHCl_3$. Because of the presence of strong π–π intermolecular interactions, it is quite unlikely that C132-C_{16} molecules detach from the fibers and get dissolved in the surrounding, disordered PDI layer. In addition, the occurrence of a major dissolution of C132-C_{16} in $CHCl_3$ can be neglected, as it would lead to a significant disruption of the fibers. Besides the changes on the (sub-)molecular scale, the density of the fibers and their distribution was unchanged upon the PDI deposition. The fibers' cross-sections do not decrease, as would be expected in the case of partial dissolution, but rather they increase, thus suggesting that some PDI is adsorbed on the fibers, probably due to a strong interaction between acceptor and donor, forming a PDI external coating to the inner C132-C_{16} fibers. It is fair to note that our data does not enable us to propose a precise interpretation on both the presence of PDI within the fibers and the nature of the C132-C_{16}–PDI interaction.

Nevertheless, the presence of a significant difference in surface potential between the fibers and the surrounding layer, as detected by KPFM, confirms that, although one cannot neglect an intimate blending between the two phases, the fibers

retain a donor-type character with respect to the acceptor-type character of the layer, and thus a difference in the electrical characteristics of the two phases is maintained. This aspect is significant for device applications. Solution processing of donor–acceptor blends has been successfully used to fabricate high-efficiency solar cells, and internal order of the two phases is fundamental for high charge mobility, especially for positive charges,[45] but in the case of polymers only short-range order can typically be achieved.

In case of C132-C_{16}–PDI, the results obtained demonstrate that by exploiting supramolecular self-organization it is possible to produce blends that convey an electron-donor phase arranged in columnar architectures with lengths on the micrometer scale. These assemblies should endow an efficient charge mobility, as confirmed by pulse-radiolysis time-resolved microwave conductivity technique for various discotic PAHs.[26] Although the thickness of the blend fabricated in this way is too small to be employed in a real device, we believe that this approach can be useful for the fabrication of complex systems having high interdigitation and long-range supramolecular order.

The different thickness of the fibers in the neat films and in the blend (see above), indicating that the latter are covered by a thin layer of PDI, is in accordance with the change in the workfunction, determined by the interaction between the two molecular components. However, it should be pointed out that the resolution and accuracy in the KPFM results, in particular in the quantitative estimation of the workfunctions, could suffer from the long-range nature of electrostatic forces used to map a surface. This is because the measured potential is actually a weighted average over the potential distribution on the surface, the derivatives of the capacitances being the weighting factors.[46] Thus, care has to be taken in the quantitative interpretation of the results obtained, especially when dealing with measurements on nanoscale architectures. In our case, a non-negligible contribution to the observed decrease of 0.5 eV in the workfunction difference between C132-C_{16} and PDI can be ascribed to long-range forces averaging the measurement on a scale larger than the isolated nanostructure of interest.

KPFM qualitative measurements on heterojunctions were previously performed both on fullerene–polymer[23] and on polyfluorene-based blends[22] with a sub-micrometer lateral resolution. These samples were several tens of nanometers thick, whereas our case consisted of 5–10 nm thick films. For organic semiconductor films a few nanometers thick, the normal Mott–Schottky models are not applicable, and the conventional concepts of conduction and valence band, band bending, and Fermi level alignment cannot be assumed a priori. In such cases, surprising new behavior can be observed.[13] Nevertheless, a deep understanding of the electronic structure of the organic material is fundamental both to maximize the photovoltaic efficiency of the blend and to improve charge injection in hybrid organic–inorganic interfaces. Our case is particularly complicated owing to 1) the thickness of the supramolecular species being below 10 nm,[47] 2) the incomplete coverage of the substrate, and 3) the complex electronic nature of our assemblies, characterized by π–π stacked discs, which is even likely to be perturbed by the interaction with the substrate. The results presented here show that, although the morphological and chemical composition of the surface is not uniform on the sub-micrometer scale, KPFM makes it possible to generate a map of the surface potential with a resolution on the tens-of-nanometers and tens-of-millivolts scale. KPFM also enables the changes of this potential, determined by chemical treatments or co-deposition of other molecules, to be followed. While the present work has focused on "static" systems, a fascinating application of KPFM involves the exploration of dynamic systems, for example, the real-time study of the local electronic properties of a photoactive device during an induced current flow[20] or light exposure.[22, 23] In this way KPFM can map, in real time, the changes in the potential due to photocurrent or current bottlenecks, and follow their evolution with time.[48]

It is noteworthy that the formation of C132-C_{16} fibers and the regularity of their cross-sections on the micrometer scale indicates a reasonably high degree of order of the molecules on the substrate at the supramolecular level, which has to be compared to that obtained with more complex methods involving low-speed, high-cost vacuum processing, such as thermal evaporation or molecular beam epitaxy. In general, both the fibers and the blend described above were obtained using a simple, cheap, and up-scalable solution-processing scheme. The complexity of the supramolecular structures obtained, the high surface contact area between the A and D phases, the continuous percolation path existing in both phases, and the simplicity and high speed of fabrication of such supramolecular assemblies makes them promising systems for further research and technological applications.

Conclusions

We compared the structural and local electronic properties of monocomponent assemblies at surfaces of an electron acceptor and a donor PAH with those of the blend ultrathin film. In the latter, the self-organization into nanoscale phase-segregated architectures was accomplished by exploiting the different solubility of the molecules. KPFM revealed that each component in the blend film possesses significantly different nanoscale electronic properties from its neat film. This is due both to the intimate interactions between the two components and also the molecular order within the nanostructure self-assembled at the surface. A non-negligible role, which limits the spatial and potential resolution, has to be ascribed to the long-range nature of the electrostatic interactions employed to map the surface by KPFM. In the framework of future molecular optoelectronics applications, the results obtained for the C132-C_{16}/PDI system achieves a deeper understanding of charge exchange and transport processes in quasi-two-dimensional systems.

Experimental Section

The C132-C_{16}-PDI heterojunction was prepared in a simple two-step procedure. First, a freshly cleaved mica substrate was dipped for 5 min in a 5×10^{-7} mol L^{-1} solution of C132-C_{16} in TCB heated at 160 °C. The mica sample was then kept at room temperature for 3 h to allow the fibers to form, and then complete solvent evaporation was attained by mild nitrogen flux. Second, a 10^{-3} mol L^{-1} solution of PDI in $CHCl_3$ was spin-coated at room temperature on such a film. For the sake of comparison, neat films of the two molecular systems were also prepared by simply depositing either C132-C_{16} or PDI on freshly cleaved mica substrate.

C132-C_{16} was deposited by dipping a mica substrate for 5 min in a 5×10^{-7} mol L^{-1} solution of C132-C_{16} in TCB at 160 °C. The sample was left in the solution at room temperature for 3 h to allow fiber formation. A complete evaporation of the solvent was attained by drying-up the film using a gentle N_2 flow. The PDI sample was prepared by spin-coating a 10^{-3} mol L^{-1} solution of PDI in $CHCl_3$ at room temperature on mica. Reagent grade solvents were used. The sample morphologies were studied by noncontact SFM, using a Thermomicroscope Autoprobe CP Research. The average width of the C132-C_{16} fibers was determined taking into account the tip broadening using the model described in ref. [36].

The electronic characterization was performed by KPFM,[10,49] after calibrating the tip on a freshly cleaved graphite substrate. All samples were electrically grounded using silver paste. The KPFM measurements were performed connecting the Autoprobe CP to a Lock-in Amplifier (Stanford Research Systems, S3830), acquiring simultaneously topography and contact potential. In this setup, the cantilever is excited by a piezo at its resonance frequency ($f \approx 45$ kHz) and the shift in resonance peak is used to follow surface topography in the typical noncontact mode. At the same time, a voltage V_{ac} of amplitude between 1 and 3 V was applied to the tip. Highly conductive Si-doped cantilevers (ULNC type, resistivity amounts to 0.001 ohm cm) were used. The frequency ω_{el} of the V_{ac} voltage was kept very different from f, typically it was below 15 kHz. In the presence of electrostatic interactions due to tip–sample potential differences, an additional oscillation at frequency ω_{el} was detected on the cantilever through the photodetector of the instrument, isolated from the concomitant topography oscillation at f using the lock-in and sent to an electronic feedback. The feedback nullified this electrostatic interaction by applying an additional V_{dc} voltage to the tip. The V_{dc} signal was visualized as the KPFM signal. For more details about KPFM and applications, see ref. [11].

In this way, the workfunction (ϕ) of the two materials was determined directly from the contact potential difference detected by the KPFM on the fibers or the layers, averaging many measurements taken on different sample areas. Although for the sake of clarity we have reported only results obtained with a given KPFM tip, measurements were performed using different tips. Owing to the small size ($\approx$10 nm) of the silicon tip apex, its irregular shape and the presence of a native oxide layer, the workfunction of each tip, thus the tip–sample potential difference differs for each tip employed. For this reason, the absolute workfunction value of the Si tip, determined with respect to a reference sample, can be very different from the theoretical workfunction value of silicon, up to values of $\pm$500 mV. To account for this variability, each tip was calibrated on a freshly cleaved graphite substrate before each measurement, and its effective workfunction obtained from this calibration. In this way, even if the raw KPFM signals measured with different tips on the same sample are different, the estimated absolute values will be the same, as they are obtained by subtracting the measured tip workfunction. All the KPFM measurements were performed using calibrated tips.

Acknowledgements

We acknowledge financial support from ESF-SONS-BIONICS, the EU through the IP-NAIMO, the Marie Curie EST-SUPER (MEST-CT-2004–008128) and ForceTool (NMP4-CT-2004–013684) as well as the bilateral program CNR-CNRS.

Keywords: donor–acceptor systems · electron transport · electrostatic interactions · nanostructures · solar cells

[1] R. H. Friend, R. W. Gymer, A. B. Holmes, J. H. Burroughes, R. N. Marks, C. Taliani, D. D. C. Bradley, D. A. Dos Santos, J. L. Brédas, M. Lögdlund, W. R. Salaneck, *Nature* **1999**, *397*, 121.
[2] S. R. Forrest, *Nature* **2004**, *428*, 911.
[3] M. Van der Auweraer, F. C. De Schryver, *Nat. Mater.* **2004**, *3*, 507.
[4] C. J. Brabec, N. S. Sariciftci, J. C. Hummelen, *Adv. Funct. Mater.* **2001**, *11*, 15.
[5] J. Nelson, *Curr. Opin. Solid State Mater. Sci.* **2002**, *7*, 87.
[6] C. W. Tang, *Appl. Phys. Lett.* **1986**, *48*, 183.
[7] G. Yu, A. J. Heeger, *J. Appl. Phys.* **1995**, *78*, 4510.
[8] J. J. M. Halls, C. A. Walsh, N. C. Greenham, E. A. Marseglia, R. H. Friend, S. C. Moratti, A. B. Holmes, *Nature* **1995**, *376*, 498.
[9] W. R. Salaneck, S. Stafström, J. L. Brédas, *Conjugated Polymer Surfaces and Interfaces: Electronic and Chemical Structure of Interfaces for Polymer Light Emitting Devices*, Cambridge University Press, Cambridge, **2003**.
[10] M. Nonnenmacher, M. P. Oboyle, H. K. Wickramasinghe, *Appl. Phys. Lett.* **1991**, *58*, 2921.
[11] V. Palermo, M. Palma, P. Samorì, *Adv. Mater.* **2006**, *18*, 145.
[12] H. Takano, J. R. Kenseth, S. S. Wong, J. C. O'Brien, M. D. Porter, *Chem. Rev.* **1999**, *99*, 2845.
[13] H. Ishii, N. Hayashi, E. Ito, Y. Washizu, K. Sugi, Y. Kimura, M. Niwano, Y. Ouchi, K. Seki, *Phys. Status Solidi A* **2004**, *201*, 1075.
[14] C. Sommerhalter, T. W. Matthes, T. Glatzel, A. Jäger-Waldau, M. C. Lux-Steiner, *Appl. Phys. Lett.* **1999**, *75*, 286.
[15] X. D. Cui, M. Freitag, R. Martel, L. Brus, P. Avouris, *Nano Lett.* **2003**, *3*, 783.
[16] T. Ichii, T. Fukuma, K. Kobayashi, H. Yamada, K. Matsushige, *Nanotechnology* **2004**, *15*, S30.
[17] N. Saito, K. Hayashi, H. Sugimura, O. Takai, *Langmuir* **2003**, *19*, 10632.
[18] N. Reitzel, T. Hassenkam, K. Balashev, T. R. Jensen, P. B. Howes, K. Kjaer, A. Fechtenkötter, N. Tchebotareva, S. Ito, K. Müllen, T. Björnholm, *Chem. Eur. J.* **2001**, *7*, 4894.
[19] T. Miyazaki, K. Kobayashi, K. Ishida, S. Hotta, T. Horiuchi, H. Yamada, K. Matsushige, *Jpn. J. Appl. Phys. Part 1* **2003**, *42*, 4852.
[20] L. Bürgi, H. Sirringhaus, R. H. Friend, *Appl. Phys. Lett.* **2002**, *80*, 2913.
[21] K. P. Puntambekar, P. V. Pesavento, C. D. Frisbie, *Appl. Phys. Lett.* **2003**, *83*, 5539.
[22] M. Chiesa, L. Bürgi, J.-S. Kim, R. Shikler, R. H. Friend, H. Sirringhaus, *Nano Lett.* **2005**, *5*, 559.
[23] H. Hoppe, T. Glatzel, M. Niggemann, A. Hinsch, M. C. Lux-Steiner, N. S. Saricifti, *Nano Lett.* **2005**, *5*, 269.
[24] V. Palermo, S. Morelli, C. D. Simpson, K. Müllen, P. Samorì, *J. Mater. Chem.* **2006**, *16*, 266.
[25] C. D. Simpson, J. S. Wu, M. D. Watson, K. Müllen, *J. Mater. Chem.* **2004**, *14*, 494.
[26] M. G. Debije, J. Piris, M. P. de Haas, J. M. Warman, Z. Tomovic, C. D. Simpson, M. D. Watson, K. Müllen, *J. Am. Chem. Soc.* **2004**, *126*, 4641.
[27] P. Samorì, N. Severin, C. D. Simpson, K. Müllen, J. P. Rabe, *J. Am. Chem. Soc.* **2002**, *124*, 9454.
[28] R. Friedlein, X. Crispin, C. D. Simpson, M. D. Watson, F. Jackel, W. Osikowicz, S. Marciniak, M. P. de Jong, P. Samorì, S. K. M. Jonsson, M. Fahlman, K. Müllen, J. P. Rabe, W. R. Salaneck, *Phys. Rev. B* **2003**, *68*, 195414.

[29] J. van Herrikhuyzen, A. Syamakumari, A. Schenning, E. W. Meijer, *J. Am. Chem. Soc.* **2004**, *126*, 10021.
[30] J. J. Dittmer, R. Lazzaroni, P. Leclère, P. Moretti, M. Granstrom, K. Petritsch, E. A. Marseglia, R. H. Friend, J. L. Brédas, H. Rost, A. B. Holmes, *Sol. Energy Mater. Sol. Cells* **2000**, *61*, 53.
[31] Y. Kaneda, M. E. Stawasz, D. L. Sampson, B. A. Parkinson, *Langmuir* **2001**, *17*, 6185.
[32] K. Balakrishnan, A. Datar, R. Oitker, H. Chen, J. Zuo, L. Zang, *J. Am. Chem. Soc.* **2005**, *127*, 10496.
[33] F. Würthner, *Chem. Commun.* **2004**, 1564.
[34] R. J. Chesterfield, J. C. McKeen, C. R. Newman, P. C. Ewbank, D. A. da Silva, J. L. Brédas, L. L. Miller, K. R. Mann, C. D. Frisbie, *J. Phys. Chem. B* **2004**, *108*, 19281.
[35] L. Schmidt-Mende, A. Fechtenkötter, K. Müllen, E. Moons, R. H. Friend, J. D. MacKenzie, *Science* **2001**, *293*, 1119.
[36] P. Samorì, V. Francke, K. Müllen, J. P. Rabe, *Chem. Eur. J.* **1999**, *5*, 2312.
[37] M. Kastler, W. Pisula, D. Wasserfallen, T. Pakula, K. Müllen, *J. Am. Chem. Soc.* **2005**, *127*, 4286.
[38] H. W. Wolf, *Semiconductors*, Wiley-Interscience, New York, **1971**.
[39] V. Palermo, M. Palma, Tomovic, M. D. Watson, R. Friedlein, K. Müllen, P. Samorì, *ChemPhysChem* **2005**, *6*, 2371.
[40] M. Pfeiffer, K. Leo, N. Karl, *J. Appl. Phys.* **1996**, *80*, 6880.
[41] Moreover, further charges can be induced at the surface region of the substrate beneath the organic adlayer. Possible charge exchange between the organic film and the substrate may occur during the KPFM measurement. Nevertheless, when the tip–sample electrostatic interaction is nullified by the KPFM feedback, such an effect can be completely neglected. Under such conditions, the vacuum level of the organic adsorbate exactly coincides with that of the tip. See ref. [13], p. 1081 for more details.
[42] E. Rabani, D. R. Reichman, P. L. Geissler, L. E. Brus, *Nature* **2003**, *426*, 271.
[43] P. Müller-Buschbaum, *J. Phys. Condens. Matter* **2003**, *15*, R1549.
[44] H. O. Jacobs, H. F. Knapp, S. Muller, A. Stemmer, *Ultramicroscopy* **1997**, *69*, 39.
[45] G. Li, V. Shrotriya, J. S. Huang, Y. Yao, T. Moriarty, K. Emery, Y. Yang, *Nat. Mater.* **2005**, *4*, 864.
[46] H. O. Jacobs, P. Leuchtmann, O. J. Homan, A. Stemmer, *J. Appl. Phys.* **1998**, *84*, 1168.
[47] The thickness of our arrangements is too small for the fabrication of a solar cell prototype. Nevertheless it is helpful to understand the electronic properties of A and D blends on the nanoscale.
[48] L. Bürgi, T. Richards, M. Chiesa, R. H. Friend, H. Sirringhaus, *Synth. Met.* **2004**, *146*, 297.
[49] H. O. Jacobs, H. F. Knapp, A. Stemmer, *Rev. Sci. Instrum.* **1999**, *70*, 1756.

Received: August 29, 2005
Revised: December 19, 2005
Published online on March 10, 2006

